International Journal of Material Forming (2021) 14:547–561
https://doi.org/10.1007/s12289-020-01537-0

ORIGINAL RESEARCH

Strain path dependency in incremental sheet-bulk metal forming

S. Wernicke[1] · M. Hahn[1] · G. Gerstein[2] · F. Nürnberger[2] · A. E. Tekkaya[1]

Received: 25 October 2019 / Accepted: 9 January 2020 / Published online: 17 January 2020

Abstract
Incremental sheet-bulk metal forming (iSBMF) enables the manufacture of functional lightweight components featuring a load-adapted shape with a high material efficiency. The flexibility of the incremental forming process allows for the modification of the strain path through the adjustment of the tool motion while maintaining the final product geometry. These modifications generate both a different strain hardening and damage evolution. In this paper, a numerical and experimental investigation of the different strain paths is carried out to identify their impact on the resulting load capacity of gears. In experiments on the quasistatic load capacity of the gears it is validated that forming of gears with a strain path showing a reduced damage potential leads to a 50% higher load capacity compared to the most unfavorable strain path. Moreover, all investigated load paths present load changes that have to be taken into account in numerical modeling of iSBMF processes. Therefore, a new approach for a material characterization under multiple load changes and high effective plastic strain is tested. Compared to numerical modeling with a characterized monotonically flow curve, this approach decreases the deviation force prediction by around 80% without increasing the calculation time.

Keywords Sheet-bulk metal forming · Incremental gear forming · Strain path · Product properties

Introduction

To face the effects of climate change a radical shift in the transport sector is necessary. In particular, manufacturing processes and the lightweight potential of the components have to be improved. An improvement of material efficiency and a reduction of accelerated mass can decrease energy consumption and, therefore, environmental load. Functional components featuring gears present a great potential concerning this matter. Typically, gear components like starter gears (Fig. 1a), seat adjusters (Fig. 1b), or synchronizer rings are manufactured without a load-adapted shape, even though a high wall thickness is only necessary in the toothed area. The manufacturing of gears without a load-adapted shape is based on the restrictions of conventional processes such as fine blanking [1]. Bulk forming of gear components requires high forming forces and is limited by the load capacity of the forming press [2]. Welding of sheets with different thicknesses leads to components with weaker mechanical properties. This results in a reduced product life [3]. The milling of gear components reduces the material efficiency at the end of the value chain and does not increase the hardness of the gears. Consequently, a heat treatment is necessary afterwards. The treatment requires a subsequent descaling and causes thermal distortion. As a comparably new process, additive manufacturing of load-adapted components will not become relevant in the near future due to a long process time causing excessive costs per component [4].

Sheet-bulk metal forming [5], also known as plate forging [6], presents a promising approach for the advantageous manufacturing of load-adapted components. The advantages in this approach lie in the shortened process chain due to the process-related high effective plastic strain. Thus, the strain hardening potential of the workpiece material is utilized and subsequent hardening processes can be omitted.

Based on a locally restricted deformation zone, incremental sheet-bulk metal forming (iSBMF) enables the local adjustment of the sheet thickness and the forming of functional elements in certain areas of a component [7]. Because of the incremental procedure the deformation zone is locally

✉ S. Wernicke
sebastian.wernicke@iul.tu-dortmund.de

[1] Institute of Forming Technology and Lightweight Components, TU Dortmund University, Baroper Str. 303, D-44227 Dortmund, Germany

[2] IW - Institut für Werkstoffkunde (Materials Science), Leibniz University Hannover, An der Universität 2, D-30823 Garbsen, Germany

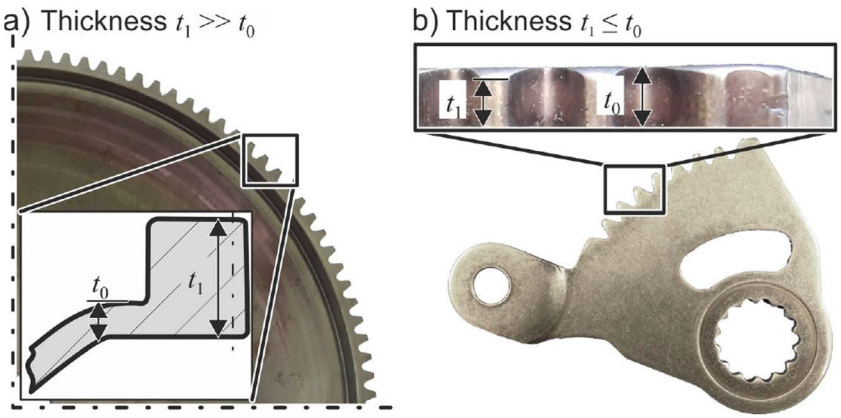

Fig. 1 **a** Edge-thickened starter gear with teeth manufactured by hobbing and **b** seat adjuster manufactured by blanking

restricted and the forming force required is many times smaller than when forming a complete gear in one stroke. This allows the forming of load-adapted components for almost any workpiece dimension. The incremental procedure is suited to form identical geometries by a variety of radial and axial tool motions [8]. Each tool motion influences the load-path and, thus, the resulting mechanical properties. Numerous works on varying load-paths in metal forming observed a significant impact on the resulting mechanical properties of the final product. It was found that the loading path during forming influences the resulting void growth within the workpiece material. McClintock [9] as well as Rice and Tracey [10] developed the first micromechanical models attributing the plastic strain-induced ductile void growth to the stress triaxiality η during forming. The triaxiality η is defined as

$$\eta = \frac{\sigma_m}{\overline{\sigma}} \tag{1}$$

Here, η is a dimensionless variable defined by the ratio of the hydrostatic stress σ_m divided by the equivalent stressσ. Triaxiality η and equivalent stress $\overline{\sigma}$ can be assigned to specific load states. During metal forming a tensional stress state ($\eta > 0$) leads to a much higher void growth than a compressional stress state ($\eta < 0$) does. Bay and Wierzbicky [11] verified that the interaction of triaxiality η and Lode parameter L affects the ductile fracture and allows for a classification of the stress state during forming. Especially small values of the Lode-parameter L reduce the formability. This permits an appraisal of the potential damage evolution.

Having the option to adjust the strain path within a process leads to the question which strain path results in the most suitable behavior in service. The focus of this paper is to determine the impact of different load-paths on the resulting load capacity of functional components. This will result in a decreased mass of accelerated components and a reduced use of materials. Additionally, changing the strain path of process steps with high tool loads offers the possibility to reduce the resulting strain hardening of the workpiece and, thus, enhances tool life. In the following, the impact of the load-path on the load capacity of the formed gear elements will be characterized by a quasistatic load capacity test. The results are evaluated based on metallographic void analyses and numerical investigations on the load-paths influenced by different tool motions. The structure of the investigations carried out is shown in Fig. 2.

Methods

This chapter introduces the different tool motions for the edge thickening of sheets and the subsequent gear forming processes. The section ends with the description of the workpiece material, the numerical model, measurement methods, and damage.

Incremental edge thickening process

Focusing on the manufacturing of components with a load-adapted shape requires an initial adjustment of the local sheet thickness. The adjustment is done by a radial displacement of the sheet material. This increases the initial thickness t_0 locally while the total volume of the sheet remains unchanged. Two different methods are possible – in-plane thickening and edge thickening (Fig. 3a). Wernicke et al. [12] investigated the in-plane thickening based on the tool indentation perpendicular to the sheet. An equivalent thickening is also achievable by a radial indenting tool motion. Sieczkarek et al. [13] investigated the so-called edge thickening on a multi-axis forming press introduced by Sieczkarek et al. [14]. This incremental procedure combined with different tool motions enables the manufacture of identical geometries featuring different strain paths. The present work focuses on different edge thickening and gear forming processes to manufacture symmetric components like gears.

Five strain paths are evaluated referring to five different process strategies with forming tools indenting radially (Fig. 3b). Starting with a continuous tool motion, a non-rotational circular tool represents the slipping edge thickening process.

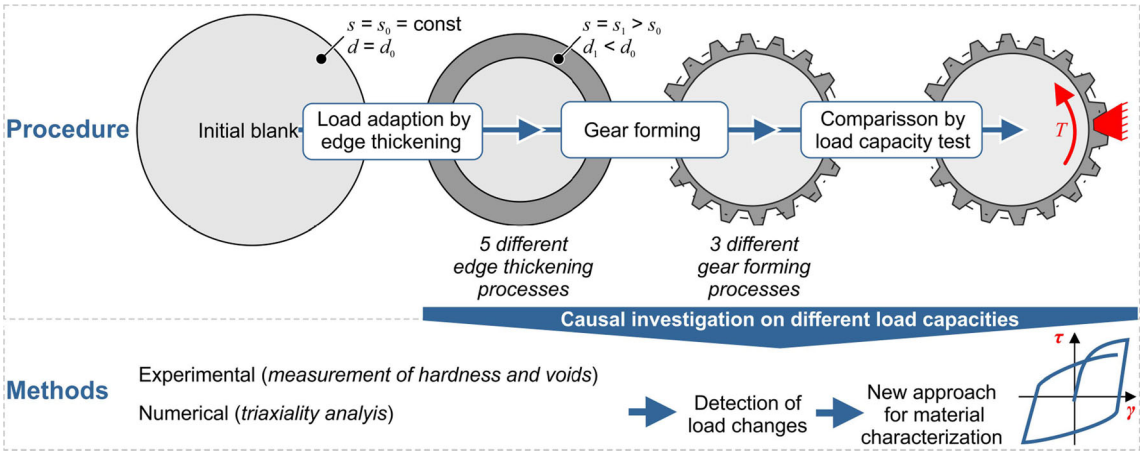

Fig. 2 Structure of the investigation and applied methods

Therefore the slipping tool indents radially while the workpiece rotates unidirectionally (ET1). As a variation, the workpiece rotates with a directional change after each rotation (ET2). In contrast, a shifting process strategy uses a free rotational forming tool indenting radially into the edge of the sheet. Here, too, the workpiece can rotate unidirectionally (ET3) or alternately (ET4). These shifting processes differ by the influence of friction. Hence, the relative velocity between tool and workpiece varies and effects the load-path. The fifth process strategy involves a clocked indenting forming tool that indents immediately following a sheet rotation (ET5). This tool motion allows for an intended material flow before and behind the forming tool. All thickening processes start with an initial sheet thickness of $t_0 = 2$ mm and a diameter of $d_0 = 106$ mm. The process ends in each case with a thickened part with a rim thickness of $t_1 = 5$ mm and a diameter of $d_1 = 96$ mm. To avoid buckling, the thickening tools indent with an increment of $i = 0.5$ mm/rev. Drylub WA 03 T (Raziol® Zibulla & Sohn GmbH) is used as lubricant.

Incremental gear forming processes

To manufacture functional components with a load-adapted shape, a subsequent gear forming process is necessary. In this process, rotational (GF1&GF2) and clocked indenting (GF3) gear forming tools form the shape of the gear (Fig. 4). For the rotational gear forming process the workpiece and the forming tool rotate either unidirectional (GF1) or they alternate (GF2). The workpiece rotates with $\omega = 240$ rev/min while the rotational speed of the forming tool is synchronized to the circumferential speed of the workpiece at the pitch cycle diameter d_f. By means of a hydraulic axis the workpiece is continuously indented with a ratio of $\Delta i = 0.5$ mm/rev. Corresponding to

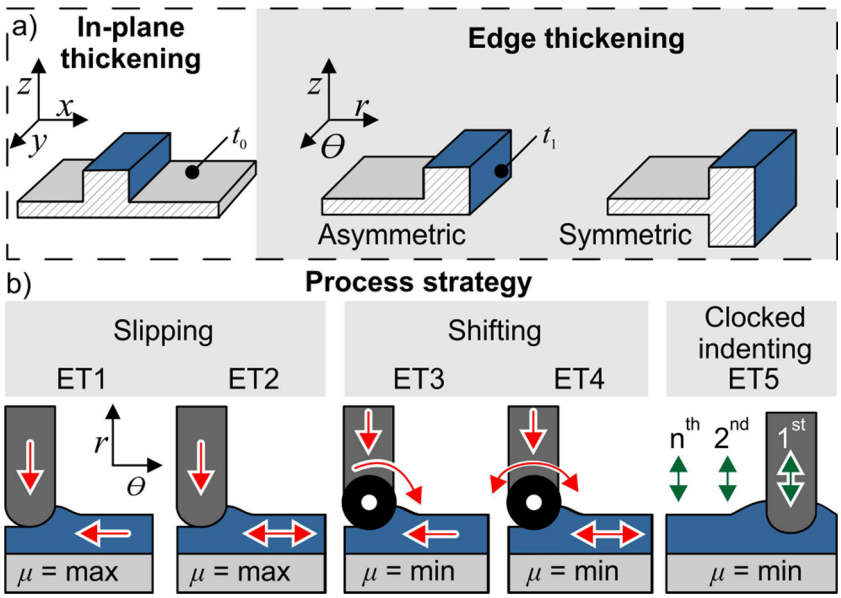

Fig. 3 Potential (**a**) adaption of the sheet thickness and **b** process strategies in incremental sheet-bulk metal forming

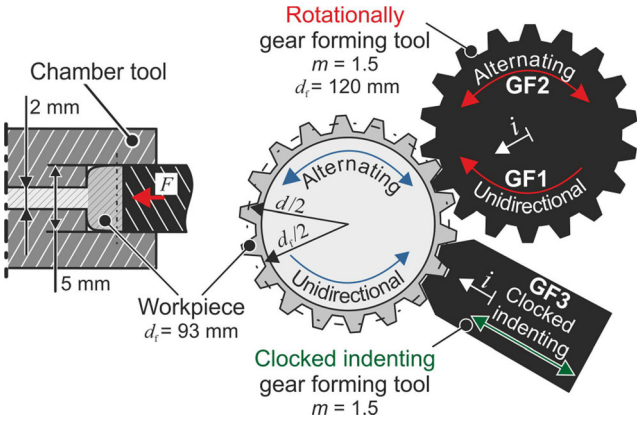

Fig. 4 Tool motions during the gear forming processes with various tool motions: GF1: Unidirectional, GF2: Alternating, and GF3: Clocked indenting

the height of a gear with modulus $m = 1.5$ mm, the maximum indentation i during both gear forming processes is set to $i = 2.25 \cdot m = 3.375$ mm.

Materials

Gröbel et al. [7] observed an effective plastic strain of $\varepsilon_{pl} > 4$ in iSBMF processes. In order to take the accompanying strain hardening effects into account, the investigated steel DC04 (material number 1.0338) with a thickness of $t_0 = 2$ mm is characterized using the in-plane torsion test described by Traphöner et al. [15]. In this study, the yield stress σ_f was determined up to an effective plastic strain of $\varepsilon_{pl} = 2.7$. The yield stress corresponding to an effective plastic strain higher than $\varepsilon_{pl} = 2.7$ is extrapolated using eq. (2) by Ludwik [16] defined as.

$$\sigma_f = \sigma_{f,0} + C \cdot {\varepsilon_{pl}}^n \tag{2}$$

($\sigma_{f,0} = 165.7$ MPa, $C = 325.4$ MPa and $n = 0.390$). All samples are manufactured by laser cutting.

Numerical modeling

The numerical investigations presented in this work are based on the commercial software Simufact Forming 15 with the implicit MARC code. The mesh is composed of hexahedron elements and a cylindrical refinement box to create elements with a minimum length of 0.25 mm for the edge thickening and the gear forming processes. A friction coefficient of $\mu = 0.15$ is used for the processes as determined by Sieczkarek et al. [17] for iSBMF of DC04 with lubrication. iSBMF of a hollow ring workpiece with an inner diameter $d_i = 60$ mm and an outer diameter $d_0 = 106$ mm was simulated resulting in a computational time of 2 to 4 weeks (4 Cores, Intel Xeon E5–2643 v3 with 3.4 GHz, 64GB RAM). A symmetry plane on half of the sheet thickness was used to reduce computation costs. In a previous work, Sieczkarek et al. [18] presented the evaluation of this model for the clocked indenting gear forming process. This numerical model enables the evaluation of the strain paths with respect to the triaxiality η during the iSBMF process.

Measurement devices

A validation of the computed strain hardening distribution is performed by means of Vickers hardness measurements with a Duramin-5 device of the company Struers. The indentation force corresponds to the Vickers hardness measurement HV0.1. Prior to the hardness measurement the workpiece is trimmed, cold-mounted, and polished. The hardness of the DC04 blanks in the initial state is determined to be $H_0 = 118.30$ HV0.1 with a standard deviation of $s_D = 2.35\%$.

Prediction and characterization of damage

To identify a potential damage evolution due to the different edge thickening and gear forming processes a numerical triaxiality strain analysis followed by an experimental analysis of the void volume fraction evolution is chosen. This allows to determine safety margins and to identify potential additional weight reductions.

The process-dependent void sizes and quantities of voids are evaluated by a metallographic investigation described by Besserer et al. [19]. Therefore, the samples are cold-mounted into a mixture of Epoxy (EpoThin) and an electrically conductive additive. This improves the quality of the imaging process in the scanning electron microscope (SEM, Zeiss SUPRA 55 VP). Voids can be measured utilizing the SEM with a total magnification of 5000x (resolution 1.2 nm) using a SE or a BSE detector. For each specimen or region of interest, an area of about 115 × 85 µm is investigated. Subsequently, the SE or BSE images were analyzed with the Software Stream Image Analysis (Olympus) to determine the number of voids and their size based on a threshold analysis. The algorithm detects voids based on differences in intensity for adjacent pixels. The determined void size depends on the number of these adjacent pixels and is based on the resolution of the image. Measurement deviations are possible based on the choice of brightness, contrast, and gamma. These parameters where kept constant to achieve consistent results. Moreover, compressive stress states can decrease the void size until they appear geometrically closed, whereas the material remains separated. Such voids cannot be detected by SEM investigations. Consequently, the real number of voids as well as the void volume fraction is usually higher than measured and can influence the load capacity of the component.

By applying this procedure to samples prepared both in sheet direction and perpendicular to the sheet direction, the void growth is evaluated spatially.

Results and discussion

This section presents the results of the investigation on the edge thickening processes followed by an analysis of the gear forming processes. First, the load capacity of the gears is measured experimentally. As a causal analysis on the varying load capacity, the strain hardening due to the forming processes is determined by hardness measurements starting with the edge thickening and later for the gear forming processes. Moreover, the load capacity is discussed considering measurements of the respective void size and void volume fraction. Along the analysis of the processes, the present strain paths and stress-strain states are compared numerically. In this comparison cyclic load changes are detected for almost all process strategies. Due to these changes, a new approach for the determination of the material behavior under cyclic loads and its numerical implementation is presented.

Quasistatic load capacity test

A load capacity test was performed for the slipping and shifting edge thickening processes. The components thickened by the clocked indenting edge thickening process have not been tested due to an inhomogeneous strain distribution that decreases the reproducibility and comparability.

The load capacity test was done using a uniaxial testing machine (Zwick Z100) enhanced by a 1000 Nm servomotor. The uniaxial movement of the traverse clamps the gear component. This clamping is mounted freely rotatable. The servomotor rotates the gear component with a velocity of $\omega_{Rot} = 0.1$ °/s. The motor is engaged with a fixed tool shaped like a gear as depicted in Fig. 5. All specimens were prepared to ensure that only one gear element is engaged. The distortion angle $\Delta\alpha$ was measured with an incremental distortion measurement unit built into a torsion device. Therefore, beside the distortion of the tooth the distortion of the support plate, the counter tool, and the fixture were also measured. This allows for a comparison based on normalized quantities. It includes a qualitative conclusion about the load capacity and distortion of the gear elements. The torque T and $\Delta\alpha$ behavior are related to the maximum measured torque T_{max} and the minimum distortion angle α_{min}. The desired product property depends on the future application of the component. Gears made for a continuous rotation, like starter gears, profit from a minimum distortion angle α_{min} at a maximum Torque T_{max}. In contrast, gears made for positioning components like seat adjusters benefit from a large distortion angle $\Delta\alpha$ at the maximum torque T_{max} based on a higher energy absorption in case of an accident.

The load capacity test reveals two different insights regarding the impact of the chosen strain path on the load capacity of the formed gears. The normalized torque T can be divided into three different sections based on the subsequent gear forming process (Fig. 5). All gears formed by the alternating rotary gear forming process fail at the highest torque. Failure at the lowest torque T was measured for the gears manufactured by the unidirectional rotary gear forming process. The load capacity of the gears formed by the clocked indenting gear

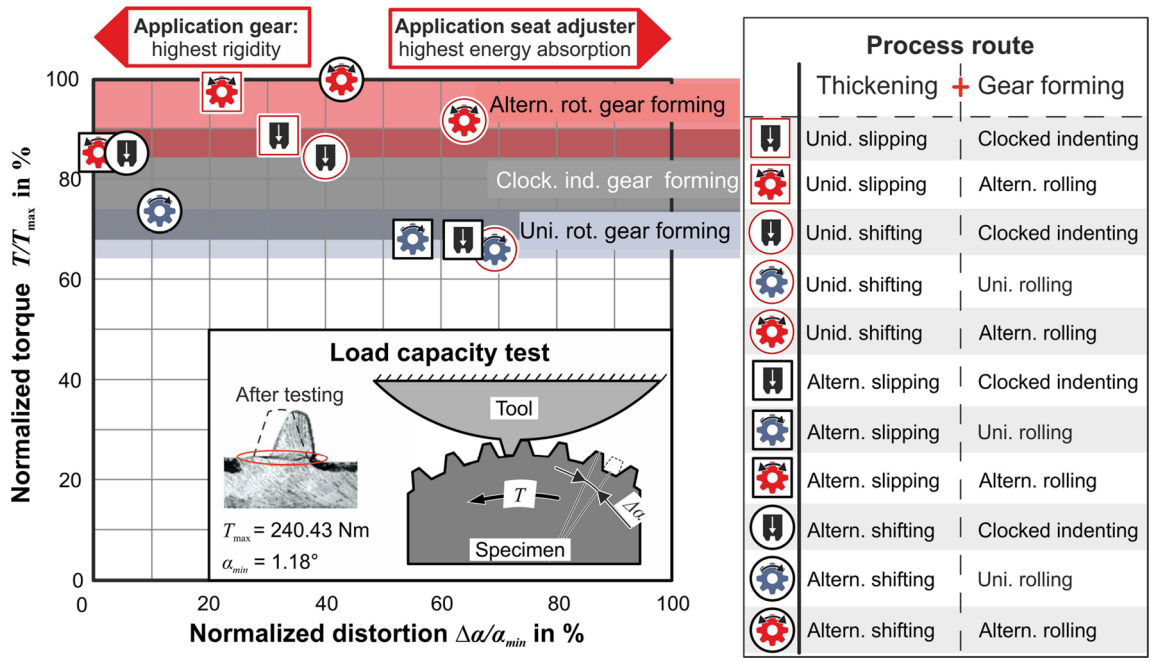

Fig. 5 Influence of the process combinations on the performance of the component. Normalized torque T and distortion $\Delta\alpha$ behavior related to the maximum measured Torque T_{max} with respect to the minimum distortion α_{min}

forming process lies in-between the other gear forming processes.

Regarding the previous edge thickening processes, the trend concerning the maximum torque T_{max} is not obvious. However, the components thickened by the alternating slipping process present 8%–20% less load capacity compared to the components thickened by the alternating shifting process. A slight impact of the edge thickening process on the distortion angle $\Delta\alpha$ is observable. Almost all gears formed by an alternating unidirectional thickening process feature a higher distortion angle $\Delta\alpha$ at the maximum torque T_{max}. While this feature is not desired for rotating gears, it is suitable for crash-relevant positioning components like seat adjusters.

Process-dependent strain distribution

The load capacity test shows that the edge thickening processes have just a slight impact on the resulting load capacity of the gears formed later. This is unexpected because a significant change of the maximum hardness can be measured at the thickened edge of the sheets (Fig. 6). Figure 6 relates the hardness increase ΔH to the initial hardness H_0 of the workpiece material. It is clear that the unidirectional edge thickening step conducted with slipping tools leads to the highest hardness increase. Conversely, the hardness increase is the lowest when using the alternating procedure and shifting forming tools.

To understand the observed hardness increase, the distribution of the effective plastic strain is analyzed numerically. Figure 7a depicts the material flow of different edge thickening processes through point tracking evaluation. For the unidirectional processes the particles at the sheet edge shift circumferentially by an angle α (Fig. 7b). In contrast, the alternating processes reverse this circumferential shift and present a lower effective plastic strain ε_{pl}. Figure 7c shows the impact of the different process strategies on the relationship between effective plastic strain ε_{pl} and the maximum observed effective plastic strain $\varepsilon_{pl,max}$.

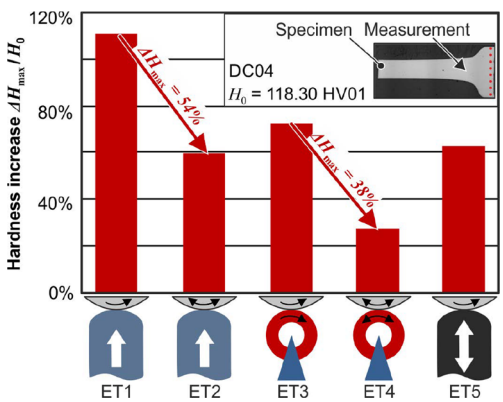

Fig. 6 Maximum of the observed hardness increase ΔH related to the initial hardness of 118.30 HV0.1

This evaluation presents a significant difference in the resulting strain hardening ε_{pl} appearing at the outermost 0.5 mm of the sheet. As a consequence, a targeted selection of the edge thickening procedure yielding a reduction of the effective plastic strain ε_{pl} of the sheet of up to 38% is possible. In the case of DC04 this means a reduced strain hardening of $\Delta\sigma_f = 6\%$. With respect to the subsequent gear forming processes, the indentation into a less strain-hardened sheet reduces the tool load and increases the tool life. Using the edge thickening process with higher effective plastic strain leads to an increased surface hardness (compare Fig. 6). Accordingly, the wear resistance of the formed gears can be improved. A missing impact on the load capacity of the gears formed later can be ascribed to the radially influenced distance that amounts to only 15% of the later tooth height.

Damage development during edge thickening

The resulting triaxiality Lode conditions during maximum strain rate $\dot{\varepsilon}_{pl,max}$ are depicted in Fig. 8. At this stage most of the considered points during all five thickening processes have a negative triaxiality η. This applies to near-surface measurements ($\Delta r \approx 0$ mm) as well as to those at a distance corresponding to the ground of the gear formed later ($\Delta r \approx 3$ mm). It signifies that most of the forming during all thickening processes occurs under a compressional stress state, which leads to a negligible damage evolution. Accordingly, the outstanding forming capacity observed during edge thickening can be ascribed to the process-characteristic compressional stress states.

While a majority of the forming occurs during a compressional stress state, a small fraction of forming occurs with a different stress state beside the main forming region. Therefore, adjacent forming regions can be in front of or behind the tool movement. Their presence depends on the tool motion and leads to different stress states during forming. The highest amount of forming in adjacent forming regions can be observed using slipping forming tools (Fig. 9a and b). In this case, the escaping material below the tool is drawn by the tool. As a consequence, the strain rate $\dot{\varepsilon}_{pl}$ increases behind the tool while also the triaxiality η rises and finally becomes positive. Therefore, damage can occur during this mostly compressional forming process.

The missing influence of friction by shifting forming tools reduces the amount of these adjacent forming regions (Fig. 9c and d). Considering the influence of an alternating tool movement presents a slightly increased strain rate $\dot{\varepsilon}$ at the outer edge ($\Delta r \to 0$). This can be assigned to locally plastic yielding based on enlarged strain hardening towards the unidirectional tool movement.

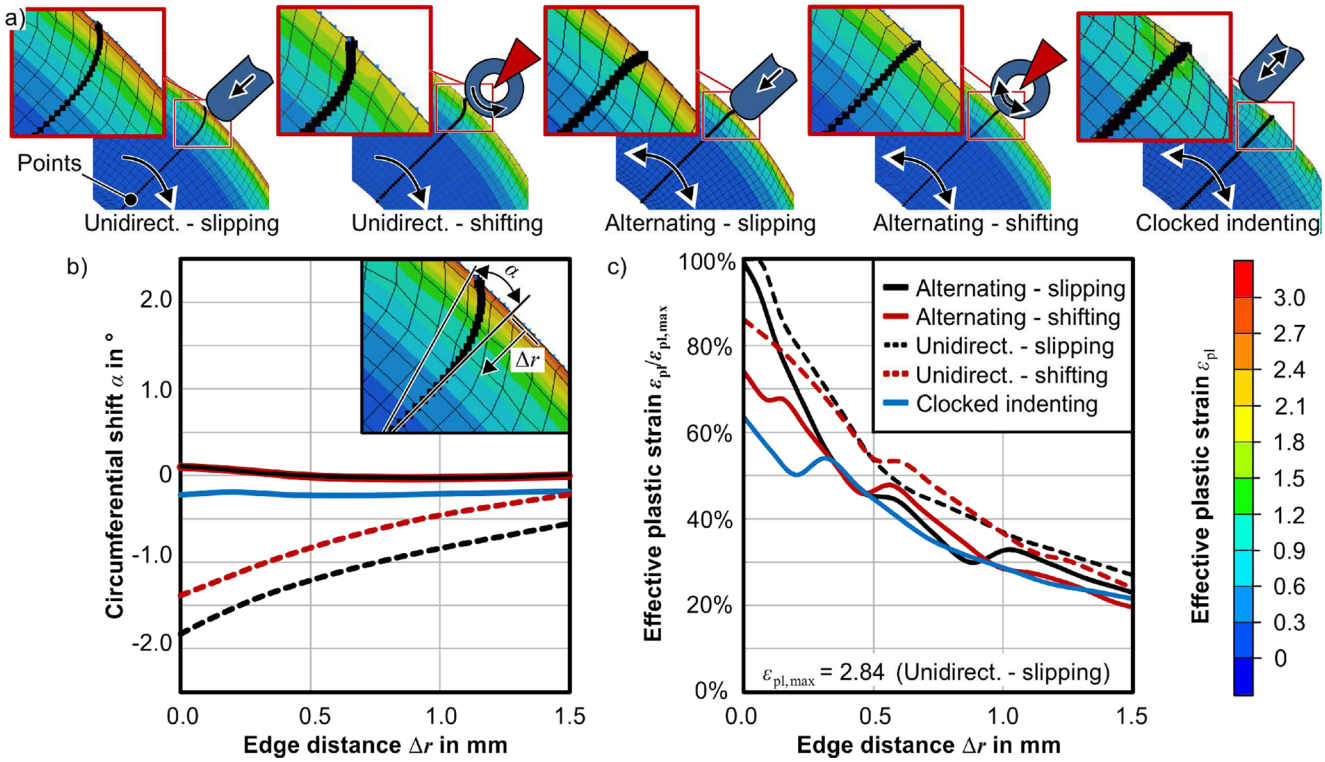

Fig. 7 **a** Shifted material shown by point tracking, **b** circumferential shift, and **c** related effective plastic strain at the sheet edge

A larger area susceptible to damage can be seen in the case of the clocked indenting edge thickening process (Fig. 9e). In this case, a much larger fraction of forming takes place with a positive triaxiality and a tensional stress state respectively. This means the clocked indenting procedure is most relevant for damage evolution during edge thickening.

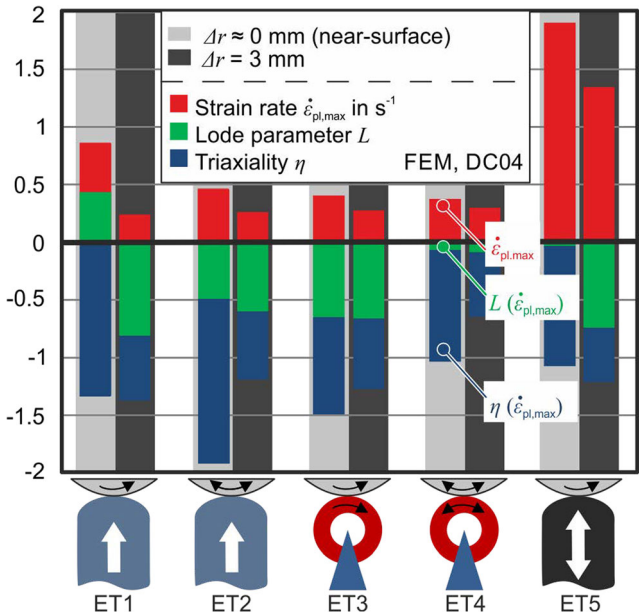

Fig. 8 Triaxiality η and Lode parameter L at the end of the different thickening processes measured in the area where the strain rate $\dot{\varepsilon}_{pl}$ is at maximum

A comparison of the stress states in the most critical forming regions, attributed to forming under highest triaxiality, is presented in Fig. 9f for all investigated edge thickening processes. The presented numerical investigation on the triaxiality Lode configuration during edge thickening gives an indication for damage evolution during the edge thickening processes. To examine the resulting damage evolution, the arising number and size of voids was investigated experimentally. The voids were measured near the radial surface ($\Delta r \approx 0$ mm) in a cross section located at half sheet thickness ($z = 0$ mm).

The results of the investigation on the void volume fraction (VVF) for the initial sheets and the thickened sheets are shown in Fig. 10 for measurements in the r- and r-z-plane. The two different planes present a different void fraction evolution. In the case of voids measured in r-plane, the averaged VVF is slightly higher for all edge thickening processes. Furthermore, the clocked indenting procedure increases the VVF by around 380%. This corresponds to the numerical investigation on the damage evolution. Expect for the alternating slipping and the clocked indenting edge thickening process, the edge thickening processes decreases the variance of the VVF. This corresponds to the triaxiality and Lode conditions shown in Fig. 8d with regard to Fig. 9.

The compressional stress state caused by the radial indenting edge thickening tool leads to a reduced VVF growth. Furthermore, this stress state can decrease the void size in the r-plane [20]. This results in a decreased VVF compared

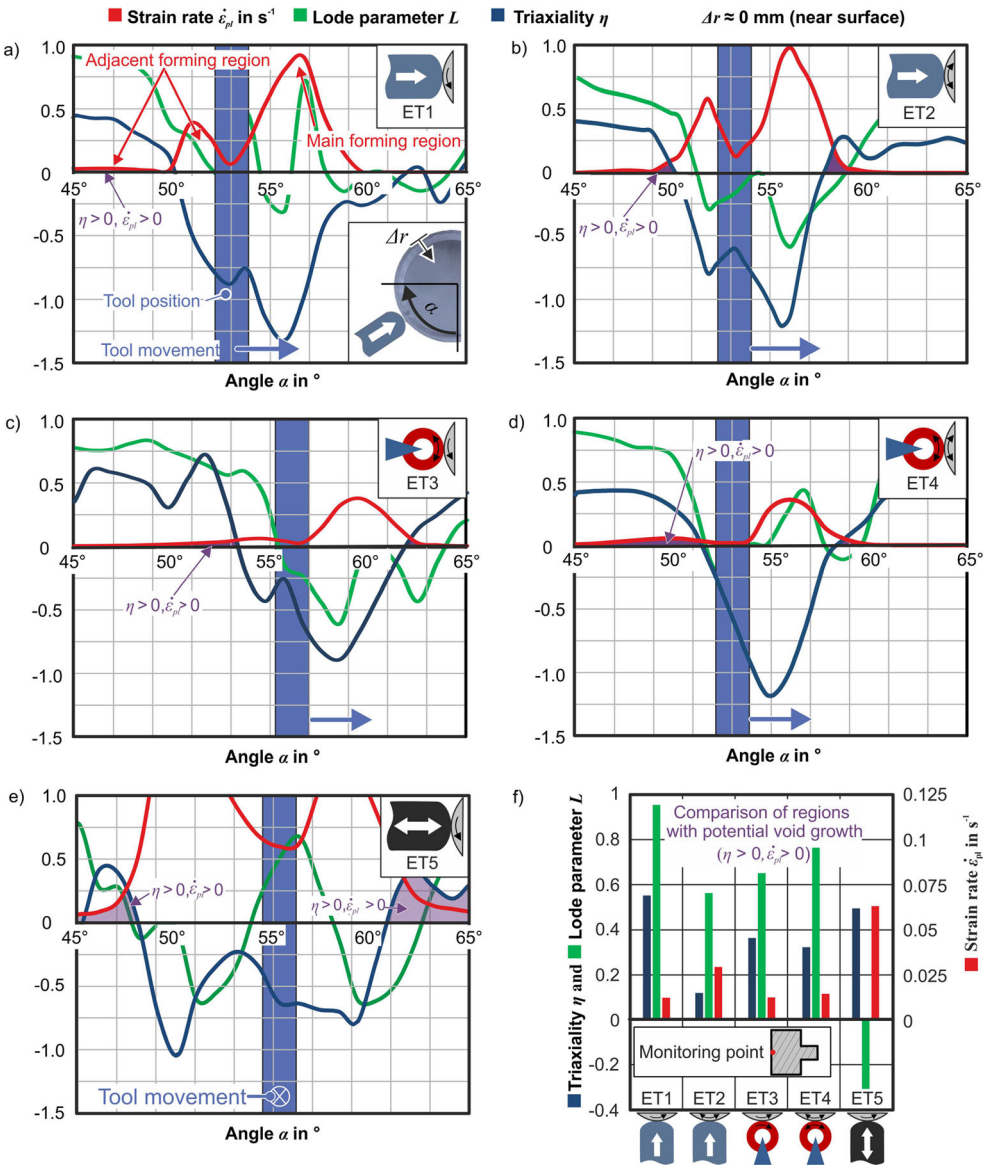

Fig. 9 Stress-strain state occurring during edge thickening using (**a**) alternating shifting, **b** unidirectional slipping and **c** clocked indenting thickening tools. **d** Comparison of the stress-strain states for the different edge thickening processes

to the initial state. The measurements in *r*-*z*-plane present a different VVF evolution. Within this plane, the material flows perpendicular to the movement of the indenting thickening tool. In *r*-*z*-plane, the slipping processes as well as the clocked indenting processes lead to the highest void growth. For the clocked indenting process the adjacent forming region where material flows with an unfavorable triaxiality Lode condition is several times larger compared to the adjacent forming regions of the other edge thickening processes. This can be one reason for the increased VVF. In the case of slipping forming tools, the adjacent forming region as well as the triaxiality-Lode conditions are not significantly different compared to those of the processes using shifting thickening tools. It is rather the 20% higher effective plastic strain that will lead to the increased VVF in *r*-*z*-plane.

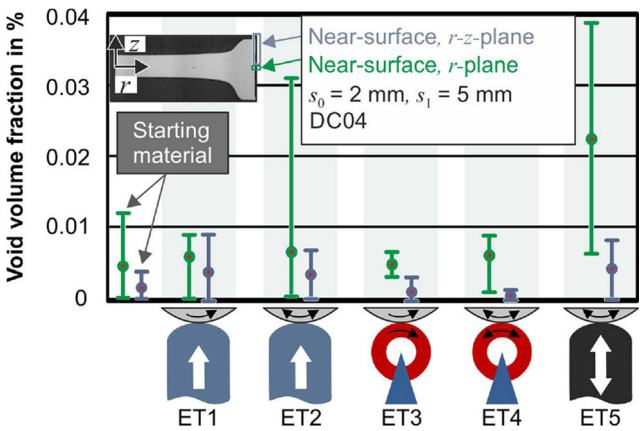

Fig. 10 Void volume fraction of a DC04 sheet after edge thickening

When discussing an edge thickening process with minimal damage evolution, the uniaxial shifting edge thickening process is at the forefront, as it appears to have the least susceptibility. Moreover, this process presents the lowest void

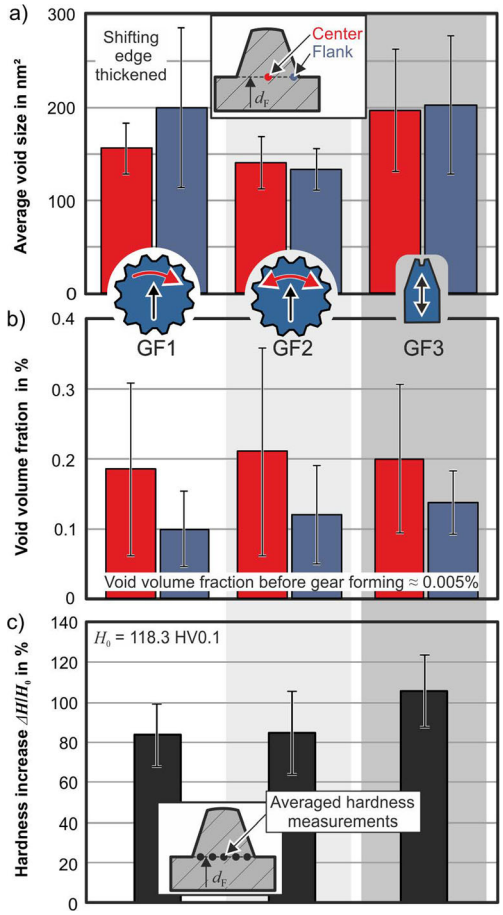

Fig. 11 Averaged (**a**) void size, **b** void-volume fraction, and **c** hardness increase at the root diameter d_f after the gear forming using different strategies

volume fraction compared to the other edge thickening processes. Therefore, the uniaxial shifting process presents the best initial condition for the manufacturing of gears by incremental sheet-bulk metal forming.

Void evolution during gear forming

The load capacity test presents a correlation between the gear forming processes and the resulting load capacity of the gears. Beside diverse hardness increases, a different damage evolution during gear forming must be considered. Accordingly, the averaged void size (Fig. 11a) and void volume fraction (Fig. 11b) were investigated for the different gear forming strategies and compared with the respective hardness increase (Fig. 11c). For this set of experiments the unidirectional shifting edge thickening process is used due to the slightest void evolution and variance (Fig. 10). The voids are measured at the center (red) and at the flank (blue) at the height of the root diameter d_f. Due to the notch effect, which influences the power deflection at the ground of the tooth flank, the void size at the flank is expected to be more relevant regarding the load capacity of the teeth. In this position the measurements are intended to display that the average void size is at lowest in gears manufactured by the alternating procedure using rotational tools (GF2). This procedure reduces the averaged void size by around 35% and decreases the variance of the resulting void size compared to the unidirectional procedure (GF1). For both processes, the averaged hardness at the level of the root diameter is almost equal. This reveals why the load capacity of the gears manufactured by the alternating procedure (GF2) is significantly higher. Between them, the load capacity of the gears manufactured by the clocked indenting procedure (GF3) is located. This can be traced back to the interaction of a higher hardness increase as well as higher averaged void size and void volume fraction (VVF).

The measured VVF obey high variances (Fig. 11b) for all gear forming processes. Because of this, the impact of the gear forming process on the VVF located at the center of the gears is not obvious. However, there is a slight tendency of the VVF to be minimum for gears formed with the unidirectional rotating gear forming process.

The investigation of the void size is in agreement with the results of the load capacity test. Comparing the VVF after edge thickening and after the gear forming of edge-thickened sheets shows that the averaged VVF doubles or quadruples during the different gear forming processes respectively. This justifies that the gear forming processes present a clearer impact on the load capacity of the teeth than the edge thickening processes (compare Fig. 5). To identify the void evolution during the gear forming processes, the processes have been analyzed numerically.

Numerical investigation on damage evolution during gear forming

For the investigation of the potential damage development during the gear forming processes several different positions in the gear are observed. Figure 12 shows the interaction of triaxiality and Lode parameter present during the gear forming process using rotational tools at the incoming flank (Fig. 12a), the center of the gear (Fig. 12b), and the outgoing flank (Fig. 12c) in the height of the later gear ground. The final stage of the forming process, consisting of the final rotation, is observed at the center of the plate. This observation uses a sheet without preceded edge thickening in order to have an isolated view on the damage evolution resulting from this process strategy. This means a free material flow in thickness direction due to the absence of contact to the chamber tools. This reduces the hydrostatic portion on the state of stress and means an upper bound in case of the damage potential.

Figure 12 represents the asymmetric triaxiality-strain path relation. This is where the increment of effective plastic strain $\Delta\varepsilon_{pl}$ along the last rotation is symmetric. At the incoming area (Fig. 12a) the forming begins with a negative triaxiality which becomes positive after 15% of the forming increment $\Delta\varepsilon_{pl}$.

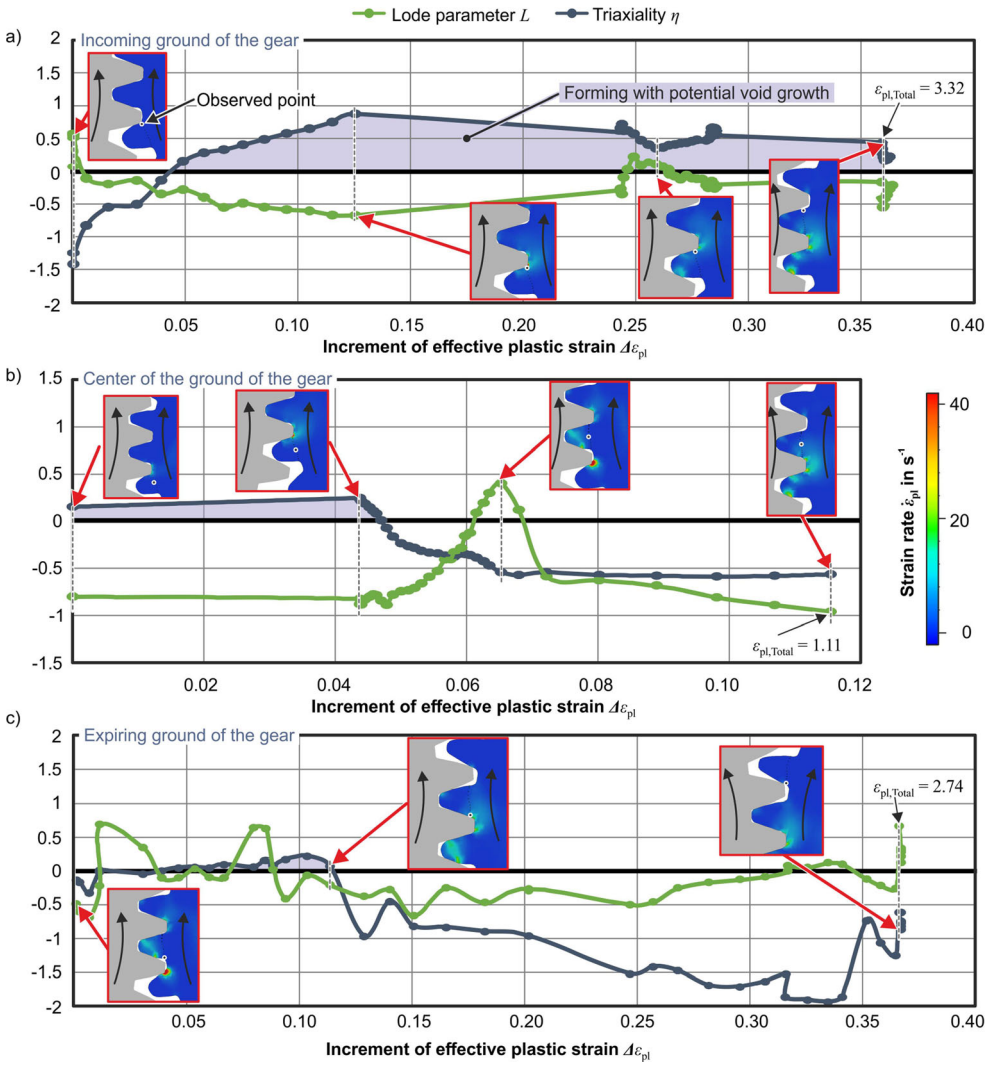

Fig. 12 Triaxiality-strain development at the ground of the (**a**) incoming flank, **b** gear center and **c** outgoing flank of the gear

After the workpiece comes in contact with the tool flank, this leads to a bending moment in the gear causing a tensional state of stress in the incoming area. Even the contact with the opposite flank does not lead to a negative triaxiality. Therefore, most of the forming at the incoming side occurs under a positive triaxiality and, thus, enables damage evolution.

At the center of the gear (Fig. 12b) 38% of the plastic strain increment $\Delta\varepsilon_{pl}$ occurs with a positive triaxiality. Here, the forming increment begins with a positive triaxiality and ends in a negative triaxiality. This reduces the potential for damage evolution.

Both the forming at the incoming and the outgoing area ends with the detachment of the incoming flank and the flank of the forming tool. At this point, the forming tool is in contact with the ground of the gear. The contact pressure exists without a significant lever and, therefore, does not cause a bending moment. The resulting negative triaxiality continues until the end of the forming increment. As such, the outgoing side of the gear presents a reduced potential for damage evolution. Furthermore, already present voids can get smaller. This triaxiality-strain path relation explains the load capacity of the gears manufactured by the gear forming process with alternating tool rotation. In this condition, each side of the gear is alternately incoming and outgoing. Over several forming increments this alternation leads to an increased amount of plastic strain under reduced damage evolution. Moreover, the alternation can increase the load capacity by decreasing the size of already existing voids.

The numerical investigation on the damage evolution of the clocked indenting gear forming process has to be divided into the forming of the first gear element and the forming of all further gear elements. Sieczkarek et al. [21] proposed such a division due to a fundamentally different material flow.

Figure 13 presents the interaction of triaxiality and Lode parameter during the increment of effective plastic strain $\Delta\varepsilon_{pl}$. During the forming of the first gear element (Fig. 13a and b) the triaxiality is always negative and, thus, a damage evolution is prevented. In contrast, the forming of the second gear

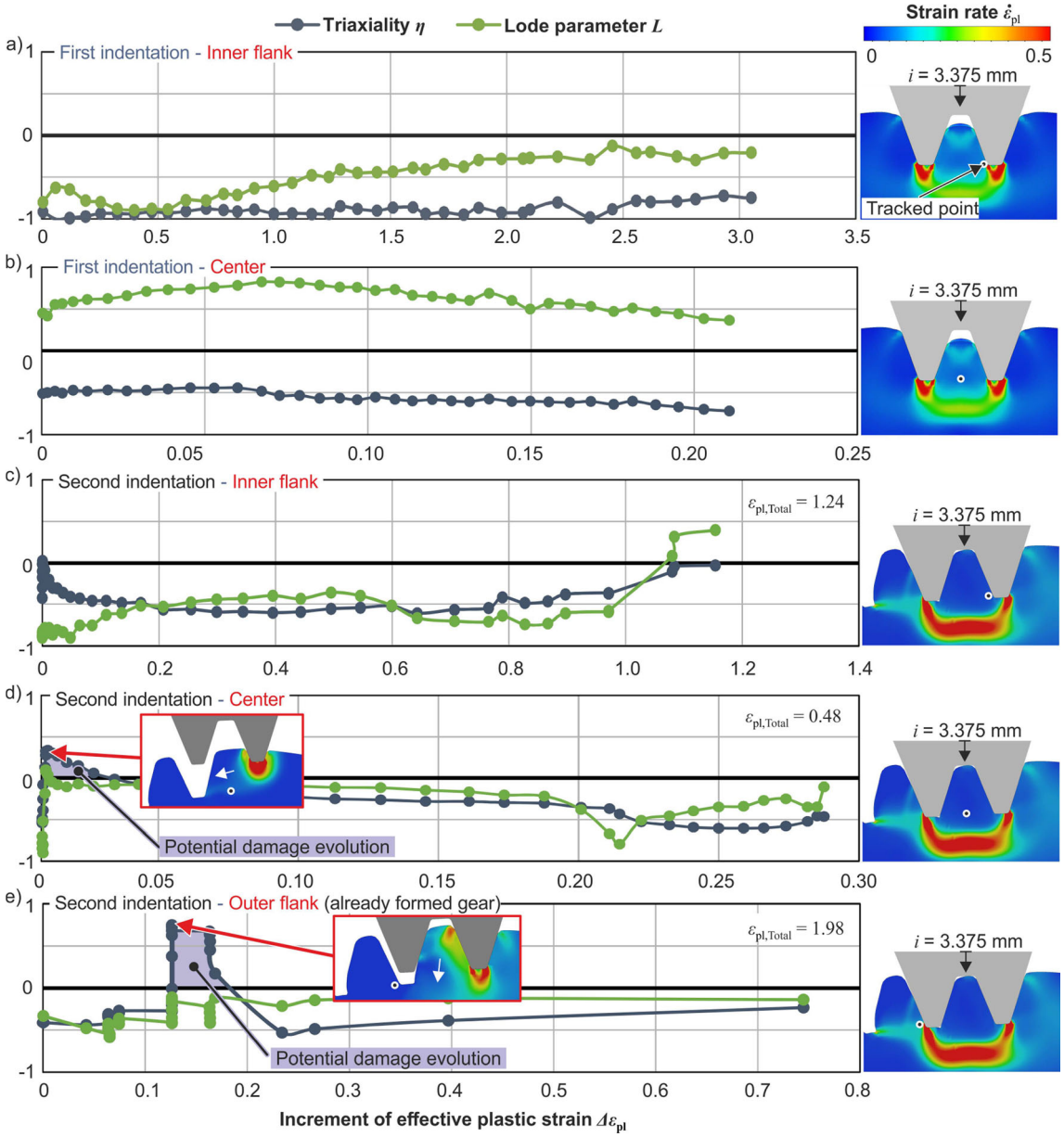

Fig. 13 Triaxiality and Lode parameter evolution during the first (**a**-**b**) and second (**c**-**e**) indentation of the clocked indenting gear forming process

element occurs with a higher triaxiality (Fig. 13c). This second gear element presents a positive triaxiality in its center (Fig. 13d) and, consequently, void growth might occur.

In the case of the center of the second gear element, the V-formation of the tool leads to a sliding and bending of gear elements. This sliding and bending stops after the tooth is in contact with the opposing tool flank. Afterwards, the forming continues under a negative triaxiality. With an increasingly filled cavity of the tool, the second formed gear element becomes a dead metal zone with its strain rate becoming zero. With the continuous feeding of the forming tool, the dead metal zone becomes shifted and causes a tensional stess state in the ground of the adjacent gear element.

When comparing the gear forming using rotational tools (GF1 and GF2) and clocked indenting tools (GF3), the effective plastic strain increment $\Delta\varepsilon_{pl}$ under potential damage evolution of GF3 is significantly smaller. This variation suggests that gears manufactured by the clocked indenting procedure have a higher load capacity when compared to those made by the unidirectional-rotational gear forming process (GF1). In the case of gears manufactured by the clocked indenting process (GF3), the effective plastic strain at the root diameter d_f, where the gears under load shear away should be substantially lower than that of the gears manufactured by rotational tools. In contrast, hardness measurements of these gears (GF3) present a much higher hardness increase than gears manufactured using rotational tools. Therefore, the observed load changes

seem to lower the strain hardening of the material and, thus, the load capacity of the gears. For this reason strain hardening corresponding to the observed effective plastic strain and number of load cycles has to be characterized and taken into account for gears manufactured by rotational tools.

Impact of load paths on material characterization and numerical modeling

The investigation on the load path during edge thickening processes demonstrated a load change for each rotation of the workpiece. The edge thickening processes require several rotations to avoid a buckling of the workpiece. Moreover, the subsequent gear forming using rotational forming tools also requires several rotations. Metals, when exposed to load changes during forming, exhibit a complex strain hardening behavior, such as the Bauschinger Effect [22]. Thus, it was chosen to investigate the influence of multiple load changes during iSBMF. Sheets were edge-thickened from a sheet thickness of $t_0 = 2$ mm to $t_1 = 5$ mm. To accomplish the unidirectional thickening process, a shifting forming tool was used. To eliminate the influence resulting from different strain rates and deformation heat, the rotational speed ω of all experiments was set to $\omega = 30°/s$, which allowed for the temperature to remain unchanged. The focus was on identifying the impact on the strain hardening behavior when having multiple load changes. The resulting radial forming force F is presented in Fig. 14a for different indentations Δi per revolution. During each revolution, the indentation occurred continuously until a revolution of 360°. After each revolution the process was stopped to ensure the correct number of 5, 10, and 50 revolutions. It is clear that decupling the number of revolutions leads to a significant reduction of the radial forming force F, while the formed geometry remains unchanged.

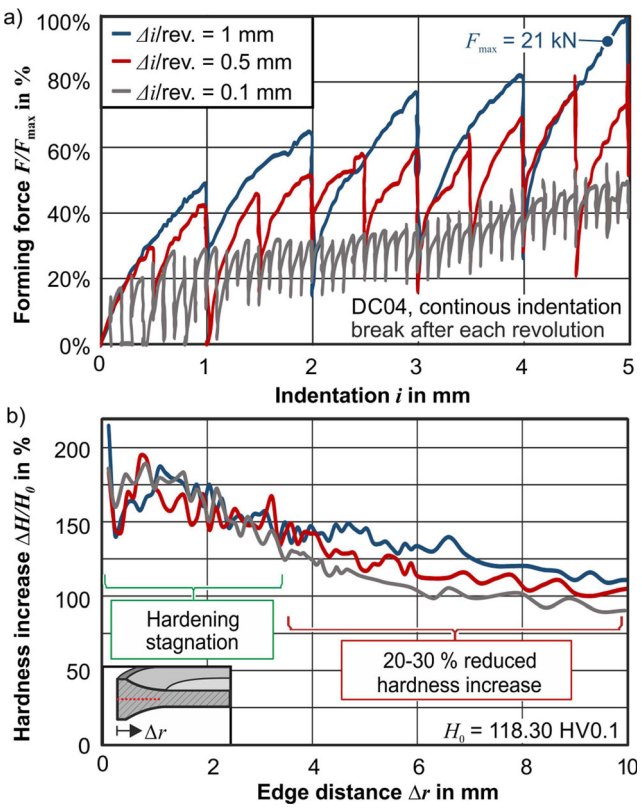

Fig. 14 Impact of varying the indentation per workpiece revolution on the (**a**) forming force and **b** resulting hardness increase ΔH

The increased forming force F is attributed to a growing deformation zone based on the increased thickness t at the edge of the sheet. Obviously, also different contact situations resulting in a variation of the indentation per revolution do not lead to a significant difference of the forming force F during the first rotation.

Measurements of the Vickers hardness (HV 0.1) after edge thickening reveal no substantially changed hardness increase ΔH in the thickened edge (Fig. 14b). However, multiple load changes reduce the strain hardening behavior as indicated by a 20–30% lower hardness increase ΔH behind the already thickened edge with the final thickness t_1. This effect is significant since the standard deviation amounts only to $s_D =$ 2.35% measured at the DC04 sheets in initial condition. This means a reduced forming force F is sufficient to continue the material flow behind the already thickened edge.

The observed dependency of load changes on the resulting forming force F lead to a deviation in numerical modeling. Using flow curves characterized under uniform loading leads to an overestimated forming force F. This impedes a realistic prediction of the resulting forming force F necessary for the machine design. Therefore, kinematic strain hardening effects have to be considered in numerical modeling. Several methods for the modeling of kinematic strain hardening effects already exist and are concluded by Chaboche [23]. While the calculation of the incremental edge thickening processes is already very computationally intensive, implementing these subroutines would increase the calculation time even more significantly. Furthermore, incremental edge thickening results in effective strains above $\varepsilon_{pl} = 2$ [7]. Thus, a material characterization representing several load changes combined with high effective strains ε_{pl} is required without making the simulation more time consuming. While the alternating tensile compression test presented by Yoshida et al. [24] is suitable for small effective strains, the unidirectional in-plane torsion test presented by Traphöner et al. [15] enables a characterization of an effective strain above $\varepsilon_{pl} = 2$. Therefore, the in-plane torsion test was used with a change of the rotational direction after small effective strains ε_{pl}. Here, the center of the sheet is clamped stationary, whereas the outer clamping rotates and applies a torque T. The samples feature a groove with a defined geometry measured by the tactile measuring system Zeiss Prismo VAST. The applied torque T leads to a calculable shear stress depending on the radial position within the groove. The displacement is measured using the digital

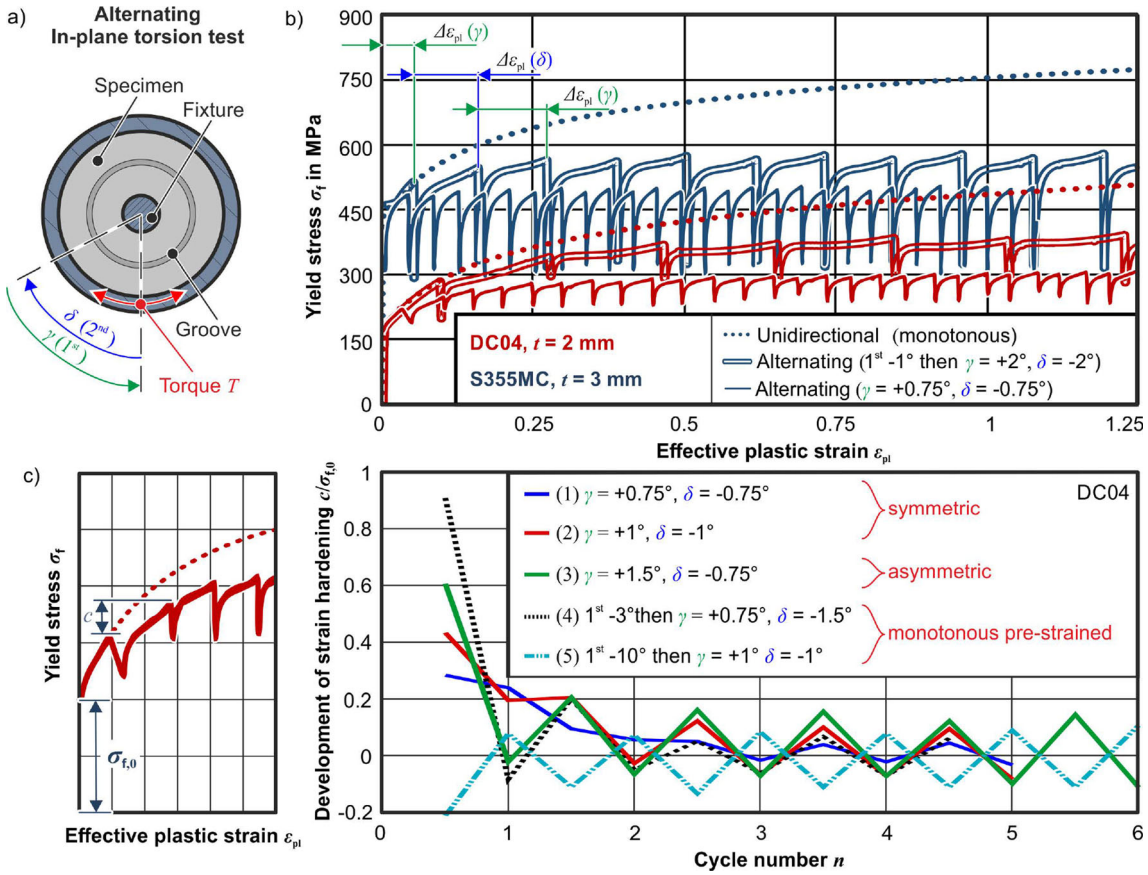

Fig. 15 **a** Procedure of the alternating in-plane torsion test and **b** resulting yield stress σ_f. **c** Impact of different amplitudes γ and δ on the resulting strain hardening increase c

imaging correlation (DIC) system Aramis by GOM. By combining the measured torque $T(r)$ and the local strain $\varepsilon_{pl}(r)$, a flow curve $\sigma_f(\varepsilon_{pl})$ can be calculated for each load cycle. Each load cycle consists of a counter-clockwise rotation by the angle γ followed by a clockwise rotation by the angle δ (Fig. 15a). The angles γ and δ were set in the machine control. Due to tolerances and an unavoidable deformation of the experimental setup, the resulting angle was smaller than configured. However, the measurement, and thus the calculated plastic strain ε_{pl}, is of sufficient precision. Because of these factors, a reduction of the angles γ and δ was limited to ±0.75°. For the second amplitude, after pre-straining with an angle of 1°, the angles γ and δ were set to ±2°. This enables an alternation around the zero position. The angle of ±2° leads to an effective plastic strain of $\Delta\varepsilon_{pl} = 0.04$ per direction and, thus, $\Delta\varepsilon_{pl} = 0.08$ per load cycle. The hysteresis flow curves known for cyclic loads discuss positive and negative strains [24]. Contrary to that, the flow curves in this investigation were plotted assuming the plastic strain ε_{pl} of each load cycle to be positive and the elastic strain ε_{el} was cleared. The investigation is conducted using the mild steel DC04 (1.0338) with a thickness of $t_0 = 2$ mm and S355 MC (1.0976) with a thickness of $t_0 = 3$ mm. Both materials are known to offer a good formability. While the investigation focuses on the DC04 steel, S355 MC is selected to validate the reproducibility of the strain path-dependent material behavior. Figure 15b presents the measured yield stress $\sigma_f(\varepsilon_{pl})$ for the different load cycles as well as the unidirectional flow curves for both materials.

The tested materials display a monotonic strain hardening behavior in the case of unidirectional shearing (dotted lines in Fig. 15b). In contrast, the alternating shearing leads to a saturation of the strain hardening behavior after the first load cycle. It can be seen that the yield stress $\sigma_f(\varepsilon_{pl})$ drops after each load change, which is typical for the Bauschinger effect [25]. Subsequent recurring load cycles do not lead to a further strain hardening. Figure 15c presents the results of the alternating in-plane torsion test for different amplitudes and a different monotonous pre-strain for the DC04 steel. The strain hardening increment c after each load is related to the initial yield strength $\sigma_{f,0}$. Changing the symmetric amplitudes of the distortion angles ($\gamma = \delta$) from 0.75° (Fig. 15c-1) to 1° (Fig. 15c-2) and 1.5° (Fig. 15c-3) shows that the amplitude of the distortion just increases the strain hardening during the first load cycle. All subsequent load cycles present an alternating strain hardening and softening behavior. Moreover, after the first two load cycles the amplitude $c/\sigma_{f,0}$ of each hardening increase and softening is proportional to the amplitude of the

distortion angles γ and δ. This behavior, averaged over several load cycles and for high effective plastic strains, leads to a stagnation of the yield stress $\sigma_f(\varepsilon_{pl})$ of:

$$\sigma_f(\varepsilon_{pl}) = \sigma_{f,0} + \frac{1}{n}\sum_{i=0}^{n} c_i \approx \text{const} = \sigma_{f,\infty} \quad (3)$$

This means materials used in iSBMF processes approximately implicate a yield stress $\sigma_f(\varepsilon_{pl})$ corresponding to the maximum yield stress $\sigma_{f,\infty}$ used for flow curve extrapolation approaches like Voce [26].

Due to the asymmetric load changes observed in iSBMF, also their impact ($\gamma > \delta$) is investigated (4). This asymmetric alternation leads to a slightly higher hardening than softening during each load cycle. It results in a slightly increasing yield strength $\sigma_f(\varepsilon_{pl})$ instead of an averaged hardness stagnation ($\sigma_{f,\infty}$ = const.). However, the increasing yield strength $\sigma_f(\varepsilon_{pl})$ under asymmetric loads is negligible compared to the one observed under monotonous loading.

Having several process routes in iSBMF means load changes can occur at different stages of the process. For this reason, also the impact of a monotonous pre-strain is investigated. These samples are pre-strained by rotation with an angle of −3° (Fig. 15c-4) and − 10° (Fig. 15c-5) before the alternation starts. These tests present the amount of pre-strain to be most relevant for the resulting yield strength $\sigma_f(\varepsilon_{pl})$. This is because of the strain hardening, which rises much faster under monotonous load. Moreover, very intensive pre-straining (Fig. 15c-5) leads to a negative strain hardening increment c already after the first load change. However, also the pre-strained material presents a strain hardening stagnation for the continuation under alternating load.

The presented strain hardening behavior under alternating loads and high effective plastic strain ε_{pl} is significantly lower than the one characterized under monotonous loading. This means flow curves determined under monotonous load and applied to simulations of iSBMF processes with cyclic load paths will lead to a significant overestimation of the resulting forming force F. Figure 16 presents the experimental and simulated force displacement curves of an edge thickening process using a slipping forming tool. The conventional simulation using a flow curve determined in the unidirectional in-plane-torsion test ($\varepsilon_{pl} < 2.7$) and extrapolation with the Ludwig approach ($\varepsilon_{pl} \geq 2.7$) leads to a forming force F_{sim} which is twice the experimental forming force F_{exp}. While the conventional simulation presents the same geometry as the experiment, the simulation cannot be used for the process design. The dashed line presents the forming force F_{sim} according to the characterization, which uses the flow curve interpolated by the maximum yield stresses $\sigma_{f,n}$ occurring at each load cycle n during the alternating in-plane torsion test. In this case the distortion γ and δ was set to ±0.75°. This is in accordance with the minimum number of load cycles realizable in the in-plane torsion test. Even if the increase of the effective strain per rotation $\Delta\varepsilon_{pl}$ does not exactly fit to the strain increments of the in-plane torsion test, the progress of the forming force F is in agreement with the one measured in the experiments.

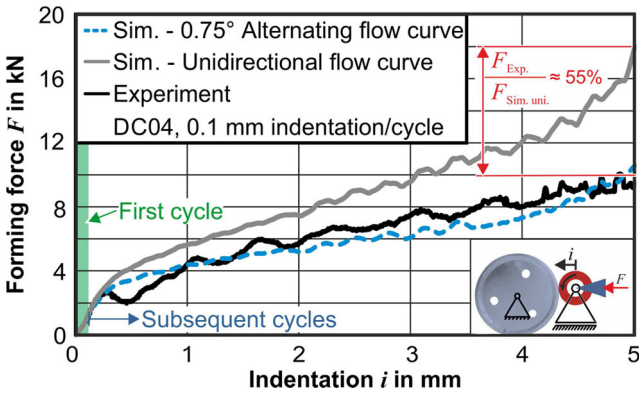

Fig. 16 Comparison of experimental and simulative forming force-indentation curves

Conclusion and outlook

Incremental sheet-bulk metal forming (iSBMF) enables the manufacturing of functional components with a load-adapted shape. The incremental procedure allows for a diversity of tool motions. This variation results in different strain paths, which is displayed by load changes with a varying degree of forming under a tensional and compressional state of stress. This led to the evaluation of process-dependent void growth during iSBMF. In opposition to the void growth during the edge thickening process, the subsequent gear forming steps show a significant influence on the load capacity of the gear elements under quasistatic loading. By considering the void growth and the quasistatic load capacity of the formed gear elements it becomes possible to identify the most suitable process strategy. For this, unidirectional edge thickening using shifting tools combined with the alternating gear forming using rotational tools is most promising.

To consider kinematic strain hardening without making the calculation more computationally intensive, a new approach is presented. This approach takes into account that the strain hardening during the in-plane torsion test with alternating loads saturates. The presented approach enables a more realistic process design without an increased numerical effort. The aim of future research work is to identify the microstructural processes influencing the strain hardening under load changes in iSBMF.

Acknowledgements We sincerely thank the German Research Foundation (DFG) for funding this work within the Collaborative Research Center SFB Transregio 73 – sub-project A4 (project number 116428118) and C4 (project number 116969364). The authors would also

like to thank Mrs. Jeanette Brandt, Mr. Kenzo Kamiya, and Mr. Heinrich Traphöner for their valuable support.

Author contributions Conceptualization, S. Wernicke., A. E. Tekkaya; funding acquisition, A. E. Tekkaya and S. Wernicke; investigation, S. Wernicke; project administration, A. E. Tekkaya and S. Wernicke; methodology, S. Wernicke and M. Hahn; validation, S. Wernicke, G. Gerstein, and F. Nürnberger; writing - original draft preparation, S. Wernicke; writing - review and editing, S. Wernicke, M. Hahn, A. E. Tekkaya, G. Gerstein, and F. Nürnberger.; supervision, A. E. Tekkaya.

Funding information Open Access funding enabled and organized by Projekt DEAL. This research was funded by the German Research Foundation (DFG), research projects A4 (project number 116428118) and C4 (project number 116969364) of the Collaborative Research Center SFB Transregio 73.

Compliance with ethical standards

Conflict of interest The authors declare that they have no conflict of interest.

References

1. Mori K, Maeno T, Tsuchiya M, Nanya T (2017) Inclusion of hot stamping operations in progressive die-plate forging of tailored high strength gear part. International Journal of Advanced Manufacturing Technologies 90:3585–3594
2. Politis DJ, Politis NJ, Lin J, Dean TA (2018) A review of force reduction methods in precision forging of axisymmetric shapes. International Journal Advanced Manufacturing Technology 97:2809
3. Gu H, Yin G, Shulkin B (2011) Laser beam welding of nitride steel components. Phys Procedia 12:40–45
4. Bamberg M, Sviridov A, Weisheit A, Schleifenbaum JH (2017) Case studies on local reinforcement of sheet metal components by laser additive manufacturing. Metals 2017(7):113
5. Merklein M, Allwood JM, Behrens B-A, Brosius A, Hagenah H, Kuzman K, Mori K, Tekkaya AE, Weckenmann A (2012) Bulk forming of sheet metal. CIRP Ann 61:725–745
6. Mori K, Nakano T (2016) State-of-the-art of plate forging in Japan. Prod Eng 10:81–91
7. Gröbel D, Schulte R, Hildenbrand P, Lechner M, Engel U, Sieczkarek P, Wernicke S, Gies S, Tekkaya AE, Behrens B-A (2016) Manufacturing of functional elements by sheet-bulk metal forming processes. Prod Eng 10:63–80
8. Wernicke S, Sieczkarek P, Gies S, Tekkaya AE (2019) Properties of components with incrementally formed gears. Metals 9:515
9. McClintock FA (1968) A criterion for ductile fracture by the growth of holes. J Appl Mech 35(2):363–371
10. Rice JR, Tracey DM (1969) On the ductile enlargement of voids in triaxial stress fields. J Mech Phys. Solids, 17 (1969), Pergamon Press, Great Britain, pp 201–217
11. Bay Y, Wierzbicki T (2008) A new model of metal plasticity and fracture with pressure and lode dependence. Int J Plast 24: 1071–1096
12. Wernicke S, Sieczkarek P, Weddeling C, Martins PAF, Tekkaya AE (2016) Local sheet thickening by in-plane swaging. Int J of Mech Sci 119:59–67
13. Sieczkarek P, Isik K, Ben Khalifa N, Martins PAF, Tekkaya AE (2014) Mechanics of sheet-bulk indentation. Journal of Materials Processing Technology Vol 214(11):2387–2394
14. Sieczkarek P, Kwiatkowski L, Tekkaya AE (2013) Novel five-axis forming press for the incremental sheet-bulk metal forming. Key Eng Mater 554:1478–1483
15. Traphöner H, Clausmeyer T, Tekkaya AE (2019) Methods for measuring large shear strains in in-plane torsion tests. J Mater Process Technol. https://doi.org/10.1016/j.jmatprotec.2019.116516
16. Ludwik P (1909) Elemente der technologischen Mechanik. Springer-Verlag, Berlin 1909
17. Sieczkarek P, Wernicke S, Gies S, Tekkaya AE, Krebs E, Wiederkehr P, Biermann D, Tillmann W, Stangier D (2017) Improvement strategies for the form filling in incremental gear forming processes. Prod Eng Res Dev 11:623–631
18. Sieczkarek P, Wernicke S, Gies S, Martins PAF, Tekkaya AE (2016) Local forming of gears by indentation of sheets. Journal of Engineering Manufacture Vol 232(5):838–847
19. Besserer HB, Gerstein G, Dalinger A, Jablonik L, Rodman D, Nürnberger F (2016) Ion beam processing in the sample preparation for the analysis of ductile damage in deep drawing steels. Prakt Metallogr 53(4):221–236
20. Hering O, Dahnke C, Ben Khalifa N, Tekkaya AE (2018) Analysing damage evolution in cold forging by means of triaxiality and lode parameter. 8th JSTP international seminar on precision forging, 05.-08.03.2018, Nagoya, Japan, pp. 121-124
21. Sieczkarek P, Wernicke S, Gies S, Martins PAF, Tekkaya AE (2016) Incipient and repeatable plastic flow in incremental sheet bulk forming of gears. International Journal of Advanced Manufacturing Technology Vol 86(9–12):3091–3100
22. Prager W (2008) Der Einfluß der Verformung auf die Fließbedingung zähplastischer Körper. ZAMM - Zeitschrift für Angewandte Mathematik und Mechanik 15(1–2):76–80
23. Chaboche JL (2008) A review of some plasticity and viscoplasticity constitutive theories. International Journal of Plasticity 24(10): 1642–1693
24. Yoshida F, Uemori T, Fujiwara K (2002) Elastic–plastic behavior of steel sheets under in-plane cyclic tension–compression at large strain. Int J Plast 18:633–659
25. Lee M-G, Barlat F (2014) Modeling of plastic yielding, anisotropic flow, and the Bauschinger effect. Reference Module in Materials Science and Materials Engineering Comprehensive Materials Processing 2:235–260
26. Voce E (1948) The relationship between stress and strain for homogeneous deformation. J Inst Met 74(1948):537–562